Microstructure and mechanical properties of metastable solid solution copper'tungsten films

K. Thomas, A.A. Taylor, R. Raghavan, V. Chawla, R. Spolenak, J. Michler

PII: S0040-6090(17)30674-0
DOI: doi: 10.1016/j.tsf.2017.09.007
Reference: TSF 36207

To appear in: *Thin Solid Films*

Received date: 7 April 2017
Revised date: 7 August 2017
Accepted date: 6 September 2017

Please cite this article as: K. Thomas, A.A. Taylor, R. Raghavan, V. Chawla, R. Spolenak, J. Michler , Microstructure and mechanical properties of metastable solid solution copper'tungsten films, *Thin Solid Films* (2017), doi: 10.1016/j.tsf.2017.09.007

Microstructure and mechanical properties of metastable solid solution copper-tungsten films

K.Thomas [a], A.A. Taylor [a,b], R. Raghavan [a,b], V. Chawla [a,c], R. Spolenak [d], J. Michler [a,*]

[a] Empa, Swiss Federal Laboratories for Materials Science and Technology, Laboratory for Mechanics of Materials and Nanostructures, Feuerwerkerstrasse 39, CH-3602 Thun, Switzerland

[b] Materials Department, University of California Santa Barbara, 93106, USA

[c] CSIR-Central Scientific Instruments Organisation, Sector 30-C, Chandigarh-160030, India

[d] Laboratory for Nanometallurgy, Department of Materials, ETH Zurich, Vladimir-Prelog-Weg 5, CH-8093 Zurich, Switzerland

* Corresponding author

E-mail addresses: keith.thomas@empa.ch +41 58 765 62 75

aidan.a.taylor@gmail.com

rejinr@gmail.com

vipin.phy@gmail.com

ralph.spolenak@mat.ethz.ch

johann.michler@empa.ch

Keywords:

Metastable phases

Nanocrystalline nanostructure

Nanoindentation

X-ray diffraction

Copper

Tungsten

Sputtering

ABSTRACT

A combinatorial science approach is utilized to study the microstructural and mechanical properties of metastable copper-tungsten solid solutions. Lateral compositional gradient (also called composition-spread) samples were deposited by simultaneously sputtering copper and tungsten targets positioned obliquely at opposite ends of a silicon substrate. The chemical composition of the film varies continuously along its length from 12 to 45 atomic % copper and has a nominal thickness of 1 μm. Nanoindentation was performed to measure the hardness and elastic modulus of the film. Grain size and solid solution strengthening models are applied to interpret the hardness of the film, though a simple rule of mixtures is found to give a more satisfactory fit to the data. The elastic modulus of the film is consistently below that predicted by the rule of mixtures. X-ray diffraction revealed plane spacing less than that predicted by Vegard's law as well as three chemical compositions exhibiting enhanced long-range order. Transmission electron microscopy analysis confirms that the film consists of a single metastable body

centred cubic solid solution where the lattice spacing and grain size depend on chemical composition.

1. Introduction

Combinatorial science, the simultaneous preparation of many samples using a single process, drastically reduces the effort required to obtain experimental data. This approach is readily applicable to thin films deposited by physical vapor deposition. Co-sputtering is one of the simplest and earliest methods developed for preparing a combinatorial materials library [1]. Sputter targets are positioned to deliver a variable flux over a large, stationary substrate. The deposited film possesses a continuous lateral variation in chemical composition with minimal variation throughout the film thickness. Dubbed the Continuous Composition Spread (CCS) technique [2], large portions of binary and ternary phase diagrams can be covered in a single deposition through appropriate geometric arrangement of the targets and substrate. For screening applications the continuous composition spread approach is often preferable to the related discrete combinatorial synthesis (DCS) approach [3] as the likelihood of overlooking a composition of interest is reduced. The most critical consideration when implementing the CCS approach is that the film should be homogeneous within the characterization volume, so strongly localized methods are needed. As with all combinatorial approaches, rapid, automatable materials characterization techniques must be utilized to efficiently process the many sampling sites across the film.

Copper and tungsten possess strongly differing mechanical and thermal properties, usually restricting their use to quite different engineering applications. Combinations

of these two metals can be designed to exploit each of their respective strengths and develop high-performance materials. The high electrical and thermal conductivity of copper coupled with tungsten's exceptional abrasion resistance and refractory properties are effectively combined in modern arcing contacts for use in high-voltage circuit breakers, welding electrodes, and heat sinks for use in harsh environments. These parts are generally fabricated using powder metallurgy and infiltration to form a metal matrix composite in which copper and tungsten are present as chemically distinct phases. The formation of Cu-W alloys using traditional melt-based processing is not possible as the Cu-W binary materials system is immiscible across its entire range of compositions. The immiscibility of copper and tungsten can be circumvented by using fabrication processes operating far from equilibrium, enabling otherwise unachievable crystalline phases to be realized [4].

Copper and tungsten are mutually insoluble across their entire range of chemical compositions under equilibrium conditions [5,6]. The immiscibility of Cu and W has been overcome to create actual Cu-W alloys in the form of films using a number of alternative techniques including ion implantation, co-evaporation, and co-sputtering. Ion implantation has been used to achieve tungsten contents of up to 10 atomic % in copper [7], whereas vapor condensation methods like co-sputtering and co-evaporation allow for any desired composition to be realized [8–10]. Depending on the deposition conditions used, the as-deposited film can be either amorphous or a metastable solid solution.

Two metastable solid solutions have been reported in the literature: one face centred cubic (FCC) substitutional solid solution on the copper-rich side of the phase diagram [7,11] and one body centred cubic (BCC) substitutional solid solution on the

tungsten-rich side of the phase diagram [10,12]. While initial reports estimated that the BCC to FCC transition occurred between 40 and 60 atomic % copper [12], no general consensus has yet been reached. Pinpointing the transition via experimental means is challenging as an amorphous region is sometimes encountered between the two metastable solid solutions, depending on the deposition conditions used. In one case this amorphous region occupies the entire region between 30 and 80 atomic % Cu [13]. More recent publications report the transition occurring at roughly 70 atomic % Cu [14], with *ab initio* simulations placing the transition at even higher copper contents, somewhere between 77 and 79 atomic % Cu [15,16]. These simulations are based on the assumption that kinetic limitations prevent the as-deposited film from forming separate Cu and W phases models. The diffusion lengths of the deposited atoms determine which metastable solid solution is energetically favorable. As such the phase transition point is predicted to occur over a small range, depending on the deposition flux and substrate temperature.

In the case of amorphous films, a gentle annealing step results in the formation of a metastable solid solution whereas higher temperature annealing will result in complete separation into pure copper and pure tungsten phases [10,17]. For ion implanted films this phase separation has been reported to occur at annealing temperatures between 400°C and 600°C [7]. For sputtered films an exhaustive experimental study covering the entire compositional range utilized an annealing temperature of 750°C and annealing times of up to ten hours to separate metastable solid solution films into their constituent elemental phases [14].

Hardness is of upmost importance for Cu-W parts as wear-resistance and durability are essential. For this reason, most commercially relevant Cu-W alloys are on the

tungsten-heavy side of the phase diagram. This is also the region selected here for study, ranging from 12 to 45 atomic % Cu. Vapor-phase deposition techniques for combinatorial studies of structural materials have been precluded in previous studies due to a desire for the bulk mechanical properties, and not those of a thin film [18]. The use of thin films is, however, completely justified for screening experiments and investigations of compositional trends, even if the quantitative strengths achieved are superior to those obtainable in bulk materials.

Early microhardness tests of BCC solid solutions (0-50 atomic % Cu) reported a hardness maximum at 18 atomic % Cu which exceeds that of pure tungsten by nearly 30%. [9] These tests were performed using a Knoop indenter in very thick films (40-150 µm) and have not been repeated. Considering the columnar microstructure of the pure tungsten films, difficulty in obtaining fully dense tungsten films, and the potential for splitting grain boundaries with a Knoop indenter, it seems plausible that the pure tungsten film hardness was underestimated. A subsequent microhardness test performed in an amorphous film with 50 at. % Cu showed enhanced Vickers hardness over pure W, but the pure W films were noted to have a columnar porous structure with many large voids [19]. With only two compositions tested along with pure Cu and W films, insufficient data was provided to draw any conclusions about hardness trends. A third study by Zong *et al.* using nanoindentation also reported superior hardness to pure tungsten in metastable BCC solid solutions containing 9 and 21 atomic % Cu, whereas amorphous films with higher Cu content had hardness inferior to the Voigt model for rule of mixtures [13]. The low modulus of amorphous films was explained by reduced film density, but no explanation was given for the enhanced hardness in BCC solid solutions. Although the compositions at which hardness values exceed pure tungsten varied between these three consecutive

reports, substitutional solid solution strengthening is the implied mechanism for increased hardness values.

The thorough evaluation of the Cu-W materials system recently performed by Vüllers and Spolenak, however, does not indicate any hardness enhancement whatsoever to pure tungsten with the addition of copper [14]. For copper contents above 40 atomic %, the data from Zong and Vüllers is in good agreement, but between 0 and 40 atomic % the data from Zong et al. [13] is significantly higher, and in some cases double, that given by Vüllers and Spolenak [14]. This research seeks to address these discrepancies using nanoindentation to determine if enhanced hardness in tungsten is achievable through addition of copper. The contribution of various strengthening mechanisms and applicability of a simple rule-of-mixtures is discussed. X-ray diffraction and transmission electron microscopy are used to obtain microstructural information including crystallite size and lattice plane spacing. Microstructural variation as a function of chemical composition is also addressed.

2. Materials and methods

The Cu-W compositional gradient film was deposited on a 4-inch silicon (100) wafer (Semiconductor Wafer) by direct current (DC) magnetron sputtering system (Mantis Deposition Ltd, UK, Model: QPrep). The sputtering targets were copper (99.99% pure, 76.2 mm diameter × 3 mm thick) and tungsten (99.95% pure, 76.2 mm diameter × 3.18 mm thick). Prior to deposition the silicon substrate was cleaned in two subsequent 15-minute ultrasonic baths: first in ethyl acetate and then isopropanol. Pressurized nitrogen gas was used to dry the wafer before

introduction into the deposition chamber. A base pressure below 1×10^{-5} Pa was achieved prior to deposition utilizing a turbo molecular pump backed by a dry rotary pump. In order to obtain a large compositional gradient the substrate was positioned closer to the sputter targets than for a typical deposition.

The sputtering of Cu and W was carried out in a pure argon atmosphere by continuous flow of argon gas through a mass flow controller into the chamber. Both of the targets underwent an argon sputter cleaning for 10 minutes with closed shutters to remove surface contaminants before deposition onto the substrate. The sputtering parameters for Cu-W film are given in Table 1. Pure copper and pure tungsten films were deposited in addition to the composition-spread sample to be used as references. Sputtering conditions for these films were identical to those used for the composition-spread sample, but with longer deposition time to reach a film thickness of 1 μm.

X-Ray Fluorescence (XRF) was used to characterize the thickness and chemical composition of the compositional gradient film. A Fischerscope X-Ray XDV was operated at 50 kV with a spot size of 3 mm to measure a rectangular grid of 8 cm × 4 cm with 1 cm spacing between measurement points.

A Hitachi S-4800 Scanning Electron Microscope (SEM) was used to obtain all micrographs. An accelerating voltage of 1.5 keV and a current of 100 pA were used to image the sample surface at a working distance of 5 mm.

The mechanical behavior of the thin film with the compositional gradient film was studied by using a Hysitron Ubi Nanoindenter. The hardness & elastic modulus

were extracted from the load-displacement curves obtained on impinging a Berkovich tip into the films by using the Oliver and Pharr analysis [20]. Maximum loads ranging from 1 to 5 mN were used in order to restrict the penetration depths to 10% of the total thicknesses of all the films with loading/unloading rates of 0.1 mN/s and a pause time at maximum load of 10 s.

When performing X-ray diffraction (XRD) measurements on a continuous composition spread film, it is necessary that the sample area illuminated by the X-rays exhibit sufficiently small variation in chemical composition to be considered homogeneous. An ideal X-ray microdiffraction setup can be achieved using a synchrotron for intense radiation, Kirkpatric-Baez mirrors or capillary optics to achieve a point focus, and a 2D detector to simultaneously collect diffracted X-rays across a large solid angle [21]. For ternary composition spread samples a point focus is necessary, even when the compositional variation is gentle. Binary composition spread samples, however, can exhibit sufficient lateral homogeneity to permit the use of a line-focus configuration, keeping diffraction intensity high and measurement time manageable. Lab-scale diffractometers are widely available and are a good choice for such measurements. The copper-tungsten sample prepared here exhibited minimal compositional variation across its 4 cm of width, making it an ideal candidate for characterization using a line-focus setup on a lab-scale diffractometer. A Bruker Discover D8 with Cu K_α radiation was used to collect the data shown in Figure 2. Initial measurements from 13 sites centered along the sample meridian at 5 mm intervals were collected across a 2θ range from 30° to 110° with a step size of 0.2° and a collection time per step of 576 seconds. A 2° offset was used when performing the initial ω-2θ scans to suppress diffraction peaks from the single-crystalline silicon substrate. A total of 68 detailed

scans were then collected along the sample meridian at 1 mm intervals across a 2θ range from 39° to 44° with a step size of 0.025° and a collection time per step of 384 seconds. These detailed scans were collected without any offset since there are no silicon peaks present across this 2θ range.

A focused ion beam workstation (FIB, Tescan Vela) was used to produce three cross-sectional lamellae for transmission electron microscopy (TEM, FEI Tecnai F30) by the lift-out process. These three sites correspond to 15.4, 19.0, and 41.3 atomic % copper content and were selected owing to the enhanced X-ray diffraction intensity at these chemical compositions. The accelerating voltage of the ion beam was stepped down from 15 kV to 5 kV during ion polishing of the samples in order to reduce the thickness of the damage layer at the surface and minimize the energy input into the sample. The samples were left relatively thick prior to TEM analysis (~150 nm) in order to ensure that the metastable microstructure was not affected. Bright field imaging (BFTEM) and selected area diffraction of the film was performed on each of the three samples. Additionally, high angle annular dark field scanning TEM and energy dispersive X-ray spectroscopy were performed on the three samples in order to investigate the compositional uniformity of the samples through the film thickness.

3. Results

3.1. Chemical composition and surface microstructure

SEM surface micrographs across the length of the sample are shown in Figure 1(a).The faceted crystalline surface structures are largest near the

tungsten-rich side of the sample and decrease steadily in diameter with increasing copper content. The diameter of these surface structures cannot be taken conclusively as the grain size since each feature could potentially contain smaller crystalline domains. As the sample was kept under vacuum for several hours after deposition it is not expected that any significant amount of surface oxidation has occurred as the sample returned to room temperature. *ImageJ* image analysis software was used to calculate the average diameter of these surface features.

(b) displays the film thickness and chemical composition as measured by XRF. Data from the medial line is shown as excellent lateral homogeneity was achieved. This enables a line-focus rather than a spot-focus to be employed for X-ray diffraction characterization of the film. A smooth, continuous compositional gradient is present in the film, ranging from 12 to 45 atomic % Cu. The film thickness varies slightly between 850 nm in the center to 1 μm near the ends, sufficiently small variation to perform nanoindentation experiments without significant influence from the substrate.

3.2. Microstructure

The XRD scans shown in Figure 2(a) indicate that a single BCC phase with a strong (110) fiber texture. A logarithmic representation of the data is necessary to see the weak (200) and (211) peaks, which are even then only detectable where there is low copper content in the film. Another small peak whose center shifts from 35.8°-37.4° is visible. This peak is attributed to the small amount of Cu-Kβ radiation passing through the nickel filter and also corresponds to the (110) peak

of the BCC solid solution. More detailed scans of the strongly pronounced (110) peak between 39 and 44 degrees is given in Figure 2(b).

The main diffraction peak is observed to shift between the {110} peak for tungsten (40.34°) and the {111} peak for copper (43.32°) with increasing copper content. The absence of any discontinuities in peak position is indicative of a single solid solution phase with variation in average lattice parameter. Molecular dynamics simulations have been used to calculate the X-ray diffraction patterns for the similarly immiscible copper-tantalum system [22]. A continuous shift of peak positions was both predicted computationally and observed experimentally in this system, though the diffraction intensity was shown to abate with increasing concentration of solute atoms. In the copper-tungsten films presented here, three local intensity maxima are observed. As there is no significant change in film texture, it is hypothesized that these chemical compositions exhibit enhanced long-range order, leading to stronger diffraction.

The microstructure and crystalline structure of the alloy at the compositions corresponding to the three XRD diffraction maxima were investigated using Bright Field Transmission Electron Microscopy (BFTEM) and Selected Area Diffraction (SAD), as shown in Figure 3. With the exception of a thin (18 nm) layer formed at the interface between the substrate and film for the 15.4 atomic % lamella, no evidence of secondary phase formation was observed. This interface layer is thin enough not to have had any impact on either the XRD or nanoindentation data. Initial BFTEM micrographs collected at 200 kV exhibited insufficient detail, therefore the BFTEM micrographs shown in Figure 3(a) were collected several months after the lamellae were produced at 300 kV to obtain higher resolution

images and observe potential sample aging. The SAD patterns all correspond to a BCC crystal structure whose lattice parameter decreases with increasing copper content, and corresponds well to the more precise calculation of the plane spacing obtained via XRD. Multiple grains from within the film are diffracting in each SAD, though noticeably more grains, and therefore smaller grain size, are observed in the 41.3 atomic % Cu sample. All of the SAD patterns were collected using the same aperture diameter. Crucially, the TEM cross-sections confirmed that the films have deposited without porosity or grain boundary cracks; this is important for the measurement of mechanical properties via nanoindentation.

3.3. Mechanical properties

Figure 4(a) shows the change in hardness of the thin film with the compositional gradient as a function of the chemical composition while Figure 4(b) displays the reduced modulus. Values for pure copper and tungsten films are included as well. The copper film exhibited a hardness of 2.1 ± 0.1 GPa and a reduced modulus of 130 ± 5 GPa. The tungsten film exhibited a hardness of 14.5 ± 1.1 GPa and a reduced modulus of 218 ± 9 GPa. The hardness values for all compositions lay between the values for pure copper and pure tungsten, while the reduced modulus was inferior to that of pure copper across much of the investigated compositional range. Only once the chemical composition dropped below 20 atomic % copper was any improvement in modulus observed. Hardness values of the pure elemental films exceed those of their bulk counterparts, largely due to their nanocrystalline nature. In the case of copper additional contributions can arise owing to the higher elastic modulus of the silicon substrate.

4. Discussion

4.1. Microstructure

Despite the mutual insolubility of copper and tungsten under equilibrium conditions, a BCC solid solution was formed across the investigated compositional range. The (110) and (220) peaks were by far the most pronounced in the ω-2θ XRD scans, which indicates a strong texture with the closest packed planes aligning parallel to the substrate surface, as is commonly observed in sputtered films. Due to the strong texture, the preparation of TEM lamellae and collection of SAD patterns was necessary to confirm the BCC crystal structure. The lattice parameter of this BCC solid solution decreases with increasing copper content and has been observed in previous studies [13,14], but the strong variation in diffraction intensity shown here has not been previously observed. As no additional peaks appear elsewhere, it is unlikely that the variations in intensity are due to a change in texture. Instead it seems plausible that these local maxima correspond to compositions at which the diffracting crystal domains are larger. As there is little variation in temperature and deposition rate across the substrate, locally enhanced surface diffusion at select compositions is potentially responsible for larger grain size. Although these maxima do not correspond to any discrete stoichiometric relations, they are hypothesized to correspond to atomic arrangements of improved stability. Surface diffusion arguments like those presented in Chang's model for metastable phase formation [15] could be extended to account for microstructural features as well.

Local minima in the diffraction peak full width at half-maximum (FWHM) correspond to the sites exhibiting the highest diffraction intensity. Amorphous films in this compositional range [13] exhibit a FWHM of 6.5°, whereas the FWHM of these films is generally around 0.7°. At the most pronounced diffraction point a FWHM of only 0.35° is observed. The crystallite size can be calculated using the well-known Scherrer equation [23]. Modifications to the Scherrer equation exist to compensate for systematic errors [24], but they rely on using multiple XRD peaks from the same phase. Owing to the strong texture of this sample, only the (110) peak was observed with sufficient intensity to apply the classical Scherrer equation (Equation 1) for calculating the lower limit of crystallite size, seen in Figure 5(b).

$$\tau = \frac{0.9\lambda}{\beta cos\theta} \qquad \textbf{Equation 1}$$

In Equation 1 τ is the crystallite size, λ is the wavelength of radiation, β is the Full Width Half Maximum (FWHM) of the peak, and θ is the Bragg angle. There are a number of factors other than crystallite size which can contribute to peak broadening, though for this sample they are assumed to be near equivalent as the deposition was performed in a single run. The crystallite size calculated underestimates the actual grain size, but is sufficient for the purpose of relative comparisons within this sample. A strong correlation between total diffraction intensity and local minima in FWHM supports the hypothesis that larger grain size is responsible for the increased diffraction intensity.

Additional information can also be gleaned from the center position of the main diffraction peak, used to calculate the plane spacing shown in Figure 5(a). A negative deviation from Vegard's Law is observed as the plane spacing and

volume of the solid solution are less than that predicted. This is not surprising as the interatomic spacing of tungsten along the close-packed [111] direction is 2.741 Å while the spacing of Cu along the close-packed [110] direction is 2.543 Å, i.e. Cu atoms are around 7.2% smaller. Deviation from Vegard's law [25] is commonly observed in solid solutions where the constituent atoms possess significantly different lattice parameters.

After several months of storage, extensive whisker growth was observed in the 41.3% at. % Cu TEM lamella. Energy Dispersive X-Ray Spectroscopy (EDS) revealed these whiskers to consist entirely of copper. These whiskers and the lamellar spinodal decomposition of the metastable metastable BCC solid solution into distinct copper and tungsten phases can be seen in Figure 3(a). The XRD experiments on this portion of the sample were repeated to determine if separation had occurred in the sample or just the TEM lamella. No change was observed in the XRD pattern, so the phase separation only occurs when a large free surface is available and sufficient time for diffusion is provided. The separation of the metastable copper-tungsten solid solution into an oriented, layered structure is presumably related to the strong texture present in the as-deposited film. Similar microstructure through lamellar spinodal decomposition has been observed in copper-cobalt material [26]. While this phase separation is interesting when considering the long-term stability of these samples or as a potential strategy for preparing multilayer structures, it does not have any bearing on the mechanical properties of the film shortly after deposition since the metastable solid solution is still intact.

4.2. Mechanical properties

No hardness increase in tungsten films was observed through the addition of copper in this work. Prior reports of hardness enhancement are likely attributable to porosity within the pure tungsten films used for comparison [9,13,19]. Though the hardness does not exceed that of pure tungsten, there is a general trend for improved hardness with increasing tungsten content. Two approaches were followed to understand this hardness trend: first using superposition of hardening mechanisms calculated from models available in the literature and subsequently by applying a simple rule of mixtures. The well-known Tabor relationship [27] was used to convert the flow stress contributions to measured hardness by multiplying by a factor of 2.7. If the various strengthening mechanisms are assumed to be independent of one another it is sufficient to simply add the contribution of their individual effects to the hardness. The calculated hardness contribution for three models is plotted alongside the measured hardness data in Figure 6.

4.2.1. Grain size strengthening

Additional strengthening is provided by the small grain size in this film. Grain boundaries inhibit the transmission of dislocations from adjacent grains, resulting in dislocation pile-up. This is described using the Hall-Petch relationship, given in Equation 2.

$$\sigma_y = \sigma_0 + \frac{k_y}{\sqrt{d}} \quad \textbf{Equation 2}$$

In Equation 2 σ_y is the yield stress contribution of grain boundary hardening, σ_0 and k_y are the empirically determined Hall-Petch constants, and d is the

average grain size. Since the film investigated here contains more tungsten than copper and has a BCC crystal structure, the Hall-Petch constants for tungsten (H_0 = 350 kg/mm^2 , k_y = 10 kg/mm$^{-3/2}$, given in terms of hardness) [28] were used rather than those for copper (σ_0 = 30.4 MPa , k_y = 0.15 MPa*m$^{1/2}$, given in terms of yield stress) [29]. Several methods for grain size determination are possible. Firstly, the grain size can be treated as being equivalent to the crystallite size calculated using the Scherrer equation from the XRD data shown in Figure 2(b). This should be considered a lower bound of grain size and tends to overestimate the hardness contribution of grain boundaries. The surface micrographs of the sample cannot be used as the grain size as there is no guarantee that the surface features represent a typical grain within the material and not a surface oxide. The BFTEM micrographs provide another potential means for confirming the grain size, but grain boundaries were difficult to identify reliably for two of the samples as the grains are typically smaller than the lamella thickness. For these reasons the crystallite size from the XRD measurements was used for all of the following calculations necessitating grain size information [28]. At the smallest grain sizes the predicted hardness contribution approaches 35 GPa. Such high hardness is typically only observed in ceramics and other ultra-hard materials. For a metallic film, even one consisting largely of refractory material, this is an unrealistically high value for hardness. The Hall-Petch constants were determined using experimental data collected from grain sizes ranging from 100 µm down to roughly 250 nm. It is therefore suggested that the Hall-Petch constants reported in the literature are not valid at grain sizes below 100 nm. The applicability of Hall-Petch hardening is not evident in the data collected here as there is no obvious correlation between grain size and measured

hardness. There is, however, a general trend of decreasing hardness with increasing copper solute concentration.

4.2.2. Solid solution strengthening

The introduction of foreign atoms into a pure material is a common tactic for improving flow strength, as first described by Fleischer using a discrete obstacle model [30]. In the model for substitutional solid solutions, hardening is achieved through the elastic interaction energy present due to both size and modulus effects. The energy contribution due to the size difference between the solute and solvent atoms is proportional to the lattice distortion term, as calculated using Equation 3:

$$\epsilon_a = \frac{1}{a_{solvent}} \cdot \frac{\partial a}{\partial c} \qquad \textbf{Equation 3}$$

In Equation 3 the lattice distortion term ϵ_a is equivalent to the slope of lattice spacing versus solute concentration, and is typically obtained via X-ray diffraction. The lattice constant of the solvent is given by $a_{solvent}$ and c is solute concentration. Over small ranges of solute concentration it is often sufficient to use a linear approximation and treat ϵ_a as a constant. Over a larger range the relationship may deviate significantly from linearity and a higher order fit may be necessary. For this data set a second order polynomial fit was applied to the data given in Figure 2(b), with the first derivative of this fit equivalent to the lattice distortion term at each site.

The energy contribution due to shear modulus difference between the solvent and solute is also determined empirically by calculating the shear modulus of the solid solution relative to the solvent. The shear modulus effect term is equivalent to the slope of the relative shear modulus vs. solute concentration plot, as given in Equation 4:

$$\epsilon_G = \frac{1}{G_{solvent}} \cdot \frac{\partial G}{\partial c} \qquad \textbf{Equation 4}$$

Here ϵ_G is the local shear modulus change term, $G_{solvent}$ is the shear modulus of the solvent, and c is again the solute concentration. In well-characterized systems, the shear modulus of the bulk material has been measured using torsion tests performed on samples spanning the range of solute concentrations of interest. Here, where bulk torsion samples of metastable Cu-W solid solutions cannot be readily produced, the shear modulus can be calculated using the measured elastic modulus from nanoindentation and assuming that the Poisson's ratio (ν) is equivalent to that of the solvent. In the case of tungsten, ν=0.28. The relation between shear modulus G, elastic modulus E, and Poisson's ratio ν is shown in Equation 5:

$$G = \frac{E}{2(1+\nu)} \qquad \textbf{Equation 5}$$

After both the lattice distortion and shear modulus terms have been calculated, the total yield strength contribution for Fleischer's solid solution strengthening model is given by Equation 6:

$$\Delta\tau_{SS} = A \cdot G_{solvent} \left| \frac{\epsilon_G}{1+\frac{1}{2}\cdot|\epsilon_G|} - \beta \cdot \epsilon_a \right|^{3/2} \sqrt{c} \qquad \textbf{Equation 6}$$

Both A and β are empirical fitting terms, with A reflecting the magnitude of the strengthening while β reflects the relative contributions of the shear modulus and lattice spacing effects. In copper, a value for β of 3 is given, indicating that the modulus effect is the dominant hardening mechanism and that strengthening arises from interactions with screw dislocations [30]. In systems where the interaction between edge dislocations and lattice strains are dominant β takes a value between 16 and 32. The constant A is <<1, with a value of 1/700 used where no specific fitting has been performed. [31]

The applicability of solid solution strengthening models over such a broad range of compositions is not widely established. Most solid solution strengthening models account for, at most, a few atomic percent of foreign atoms. Setting β as 25 and using the standard value of 1/700 for A, a reasonable fit to the data can be obtained. While the exact trend is not closely followed, the hardness magnitude of several GPa and the decreasing hardening contribution with increasing solute content are both reflected in the Fleischer model. The total hardness, however, is less than that observed in pure tungsten. Similar softening behavior has been observed in many materials systems, particularly those with a BCC crystal structure [32]. This softening is not adequately addressed by use of the Fleischer model alone.

4.2.3. Nanocrystalline solid solution grain boundary pinning

A recent paper by Rupert et. al. [33] suggests that a new strengthening mechanism occurs in nanocrystalline solid solutions as an interaction between solutes and grain boundaries. This new mechanism was suggested based on the observation of a linear increase in yield strength with increasing solute content over a large concentration range of solute (0-20%), rather than the commonly observed square-root relationship observed in coarse-grained solid solutions. A model was derived using an approach similar to that used in the Fleischer model, but with an interaction parameter which considers global property changes rather than being limited to solute-dislocation interactions. The Rupert nanocrystalline solid solution model is given in Equation 7:

$$\Delta\tau_{nc,SS} \approx \frac{G_{solvent} \cdot b_{solvent}}{d} \cdot \left(\frac{1}{G_{solvent}}\frac{\partial G}{\partial c} + \frac{1}{b_{solvent}}\frac{\partial b}{\partial c}\right) \cdot c \qquad \textbf{Equation 7}$$

The shear modulus is given by G, d represents the grain size, b is the length of the Burger's vector, and c is the solute concentration. This model accounts for both grain size and solid solution effects and can account for softening behavior in systems where solute addition results in a drop in shear modulus, as has been observed in nanocrystalline iron and nickel with copper solutes [34]. In both of these systems, the addition of copper reduces the shear modulus. For larger grain sizes there is a strengthening effect, but for nanocrystalline samples the addition of copper results in softening. As the addition of copper to tungsten also results in a reduction in shear modulus, this model predicts a softening effect across the full range of solute concentrations. The predicted softening, however, is strongest at low solute concentrations and does not fit the data well.

4.2.4. Rule of mixtures

None of the three above literature models provided an adequate fit to the data, nor did any combination of their contributions through superposition. The strengthening mechanisms considered do not appear to operate independently for this metastable copper-tungsten solid solution. The typical Hall-Petch grain boundary strengthening mechanism does not appear to be operative, either due to excessively small grain sizes or as a result of interference from other mechanisms. Solid solution softening rather than strengthening was observed as the sample hardness decreases with increasing solute content. Though no phase separation between copper and tungsten was observed, a simple rule of mixtures was also applied to model both hardness and reduced modulus. The Reuss model [35], given in Equation 8, is typically used to represent a lower bound value of the property of interest. This model, also known as the inverse rule of mixtures, is generally used to predict elastic modulus, though it can in principle be applied to any material property of interest.

$$H_{Reuss} = \left(\frac{V_f^{Cu}}{H_{Cu}} + \frac{V_f^{W}}{H_W}\right)^{-1} \qquad \textbf{Equation 8}$$

The hardness H_{Reuss} of copper-tungsten mixtures is calculated using the respective volume fractions V_f and hardnesses H of pure copper and tungsten. This model provides a superior fit of film hardness compared to the other hardening models discussed, but systematically overestimates the reduced modulus of the film. As tungsten is elastically isotropic, the strong texture should have no impact on its elastic properties. The origin of the suppressed modulus values is unclear.

5. Conclusions

A combinatorial approach was used to deposit a copper-tungsten metastable BCC solid solution ranging from 12 to 45 atomic % copper. X-ray Diffraction (XRD) and Selected Area Diffraction (SAD) data show that a single BCC solid solution phase is present within the film. The shape, position, and intensity of the main XRD peak (110) vary continuously with copper content. Three local maxima are observed, corresponding to compositions at which larger grains have formed. The mechanical properties of the film, as determined via nanoindentation, vary with chemical composition. The hardness of pure tungsten was not improved upon by addition of copper, contrary to several previous reports, but corroborating the most recent investigations by Vüllers and Spolenak. Literature models for Hall-Petch hardening, solid solution hardening, and nanocrystalline solid solution softening were all applied in an effort to gain insight into the hardness of the film, though none provided an accurate representation of the observed hardness. In the absence of a more appropriate hardening model for the metastable copper-tungsten system, a simple rule of mixtures was applied and provides as an acceptable fit to the film hardness.

6. Acknowledgements

The research leading to these results has received funding from STEEP, a Marie Curie Action Initial Training Network (ITN) of the European Union's Seventh Framework Program FP7 under REA grant agreement number 316560. Thanks also go to Mihai Gabureac for his initial work in developing the sputtering conditions to be used for depositing these films.

7. References

[1] J.J. Hanak, The “Multiple-Sample Concept” in Materials Research: Synthesis, Compositional Analysis and Testing of Entire Multicomponent Systems, J. Mater. Sci. 5 (1970) 964–971. doi:10.1007/BF00558177.

[2] R.B. Van Dover, L.F. Schneemeyer, R.M. Fleming, Discovery of a useful thin-film dielectric using a composition-spread approach, Nature. 2655 (1998) 2653–2655. doi:10.1038/32381.

[3] X.D. Xiang, X. Sun, G. Briceño, Y. Lou, K. a Wang, H. Chang, W.G. Wallace-Freedman, S.W. Chen, P.G. Schultz, A combinatorial approach to materials discovery., Science. 268 (1995) 1738–1740. doi:10.1126/science.268.5218.1738.

[4] B. Cantor, R.W. Cahn, Metastable alloy phases by co-sputtering, Acta Metall. 24 (1976) 845–852. doi:10.1016/0001-6160(76)90051-1.

[5] P.R. Subramanian, D.E. Laughlin, Cu-W (Copper-Tungsten), in: T.B. Massalski (Ed.), Bin. Alloy Phase Diagrams, Second Edi, Materials Park, Ohio, 1991: pp. 76–79.

[6] B. Predel, Cu-W (Copper-Tungsten), SpringerMaterials - Landolt-Börnstein Database. 5d (1994) Volume 5d: Cr-Cs-Cu-Zr. doi:10.1007/b4775.

[7] a. G. Cullis, J.M. Poate, J. a. Borders, The physical state of implanted tungsten in copper, Appl. Phys. Lett. 28 (1976) 314. doi:10.1063/1.88766.

[8] N. Radir, B. Gr, D. Gracin, T. Car, Preparation and structure of Cu - W thin films, Thin Solid Films. 228 (1993) 225–228. doi:10.1016/0040-6090(93)90604-N.

[9] H.F. Rizzo, T.B. Massalski, M. Nastasi, Metastable crystalline and amorphous

structures formed in the Cu-W system by vapor deposition, Metall. Trans. A. 24 (1993) 1027–1037. doi:10.1007/BF02657233.

[10] M. Nastasi, F.W. Saris, L.S. Hung, J.W. Mayer, Stability of amorphous Cu/Ta and Cu/W alloys, J. Appl. Phys. 58 (1985) 3052. doi:10.1063/1.335855.

[11] J.M. Poate, Formation of substitutional alloys by ion implantation in metals, Appl. Phys. Lett. 25 (1974) 698. doi:10.1063/1.1655366.

[12] a. G. Dirks, Metastable solid solutions in vapor deposited Cu–Cr, Cu–Mo, and Cu–W thin films, J. Vac. Sci. Technol. A Vacuum, Surfaces, Film. 3 (1985) 2618. doi:10.1116/1.572799.

[13] R.L. Zong, S.P. Wen, F. Zeng, Y. Gao, F. Pan, Nanoindentation studies of Cu–W alloy films prepared by magnetron sputtering, J. Alloys Compd. 464 (2008) 544–549. doi:10.1016/j.jallcom.2007.10.033.

[14] F.T.N. Vüllers, R. Spolenak, From solid solutions to fully phase separated interpenetrating networks in sputter deposited “immiscible” W–Cu thin films, Acta Mater. 99 (2015) 213–227. doi:10.1016/j.actamat.2015.07.050.

[15] K. Chang, D. Music, M.T. Baben, D. Lange, H. Bolvardi, J.M. Schneider, Modeling of metastable phase formation diagrams for sputtered thin films, Sci. Technol. Adv. Mater. 6996 (2016) 1–10. doi:10.1080/14686996.2016.1167572.

[16] K. Chang, M. to Baben, D. Music, D. Lange, H. Bolvardi, J.M. Schneider, Estimation of the activation energy for surface diffusion during metastable phase formation, Acta Mater. 98 (2015) 135–140. doi:10.1016/j.actamat.2015.07.029.

[17] A. Schäfer, G. Menzel, The structural and electrical properties of Metglas and amorphous metal films, Thin Solid Films. 52 (1978) 11–21. doi:10.1016/0040-6090(78)90250-X.

[18] J. Zhao, A Combinatorial Approach for Structural Materials, Adv. Eng. Mater. 3

(2001) 143–147. doi:10.1002/1527-2648(200103)3:3<143::AID-ADEM143>3.0.CO;2-F.

[19] N. Radić, M. Stubicar, Microhardness properties of Cu–W amorphous thin films, J. Mater. Sci. 33 (1998) 3401–3405. doi:10.1023/A:1013201817300.

[20] W. Oliver, G. Pharr, An improved technique for determining hardness and elastic modulus using load and displacement sensing indentation experiments, J. Mater. Res. 7 (1992) 1564–1583. doi:10.1557/JMR.1992.1564.

[21] J. Cui, Y.S. Chu, O.O. Famodu, Y. Furuya, J. Hattrick-Simpers, R.D. James, A. Ludwig, S. Thienhaus, M. Wuttig, Z. Zhang, I. Takeuchi, Combinatorial search of thermoelastic shape-memory alloys with extremely small hysteresis width., Nat. Mater. 5 (2006) 286–90. doi:10.1038/nmat1593.

[22] C.M. Müller, S. Parviainen, F. Djurabekova, K. Nordlund, R. Spolenak, The as-deposited structure of co-sputtered Cu-Ta alloys, studied by X-ray diffraction and molecular dynamics simulations, Acta Mater. 82 (2015) 51–63. doi:10.1016/j.actamat.2014.08.066.

[23] P. Scherrer, Bestimmung der Größe und der inneren Struktur von Kolloidteilchen mittels Röntgenstrahlen, Nachrichten von der Gesellschaft der Wissenschaften zu Göttingen, Math. Klasse. 1918 (n.d.) 98–100. https://eudml.org/doc/59018#.WCG1ku1onzE.mendeley (accessed November 8, 2016).

[24] A. Monshi, Modified Scherrer Equation to Estimate More Accurately Nano-Crystallite Size Using XRD, World J. Nano Sci. Eng. 2 (2012) 154–160. doi:10.4236/wjnse.2012.23020.

[25] L. Vegard, Die Konstitution der Mischkristalle und die Raumfüllung der Atome, Zeitschrift F{ü}r Phys. 5 (1921) 17–26. doi:10.1007/BF01349680.

[26] M.G.M. Miranda, E. Estévez-Rams, G. Martínez, M.N. Baibich, Phase

separation in Cu90Co10 high-magnetoresistance materials, Phys. Rev. B. 68 (2003) 14434. doi:10.1103/PhysRevB.68.014434.

[27] D. Tabor, The Hardness of Metals, ClarendonP, 1951. https://books.google.ch/books?id=jsLRAAAAMAAJ.

[28] U.K. Vashi, R.W. Armstrong, G.E. Zima, The Hardness and Grain size of consolidated fine tungsten powder, Metall. Trans. 1 (1970) 1769–1771. doi:10.1007/BF02642027.

[29] N. Kosarev, M. Khazin, R. Apakashev, N. Valiev, Mechanical Properties of Micro- and Nanostructured Copper Films, J. Mater. Sci. Chem. Eng. 1 (2013) 7–10. doi:10.4236/msce.2013.15002.

[30] R.. Fleischer, Substitutional solution hardening, Acta Metall. 11 (1963) 203–209. doi:10.1016/0001-6160(63)90213-X.

[31] T.H. Courtney, Mechanical behavior of materials, Waveland Press, 2005.

[32] R.L. Smialek, G.L. Webb, T.E. Mitchell, Solid solution softening in BCC metal alloys, Scr. Metall. 4 (1970) 33–37. doi:10.1016/0036-9748(70)90139-0.

[33] T.J. Rupert, J.C. Trenkle, C.A. Schuh, Enhanced solid solution effects on the strength of nanocrystalline alloys, Acta Mater. 59 (2011) 1619–1631. doi:10.1016/j.actamat.2010.11.026.

[34] T.D. Shen, C.C. Koch, Formation, solid solution hardening and softening of nanocrystalline solid solutions prepared by mechanical attrition, Acta Mater. 44 (1996) 753–761. doi:10.1016/1359-6454(95)00178-6.

[35] A. Reuss, Berechnung der Fließgrenze von Mischkristallen auf Grund der Plastizitätsbedingung für Einkristalle ., ZAMM - Zeitschrift Für Angew. Math. Und Mech. 9 (1929) 49–58. doi:10.1002/zamm.19290090104.

8. Figure and Table Captions

Table 1: Sputtering conditions for Cu-W compositional gradient film

Base pressure	1×10^{-5} Pa
Sputtering gas	Argon
Gas flow rate	35 sccm
Sputtering pressure	0.22 Pa
Deposition time	3.5 hours
Cu target power	35 W
W target power	84 W
Substrate temperature	Room temperature

Figure 1: (a) SEM surface micrographs and their average surface feature diameters, exhibiting decreasing surface microstructure size with higher copper content along Cu-W compositional gradient film (b) smooth, continuous spatial variation of chemical composition and film thickness variation between 850 nm and 1000 nm as measured by XRF

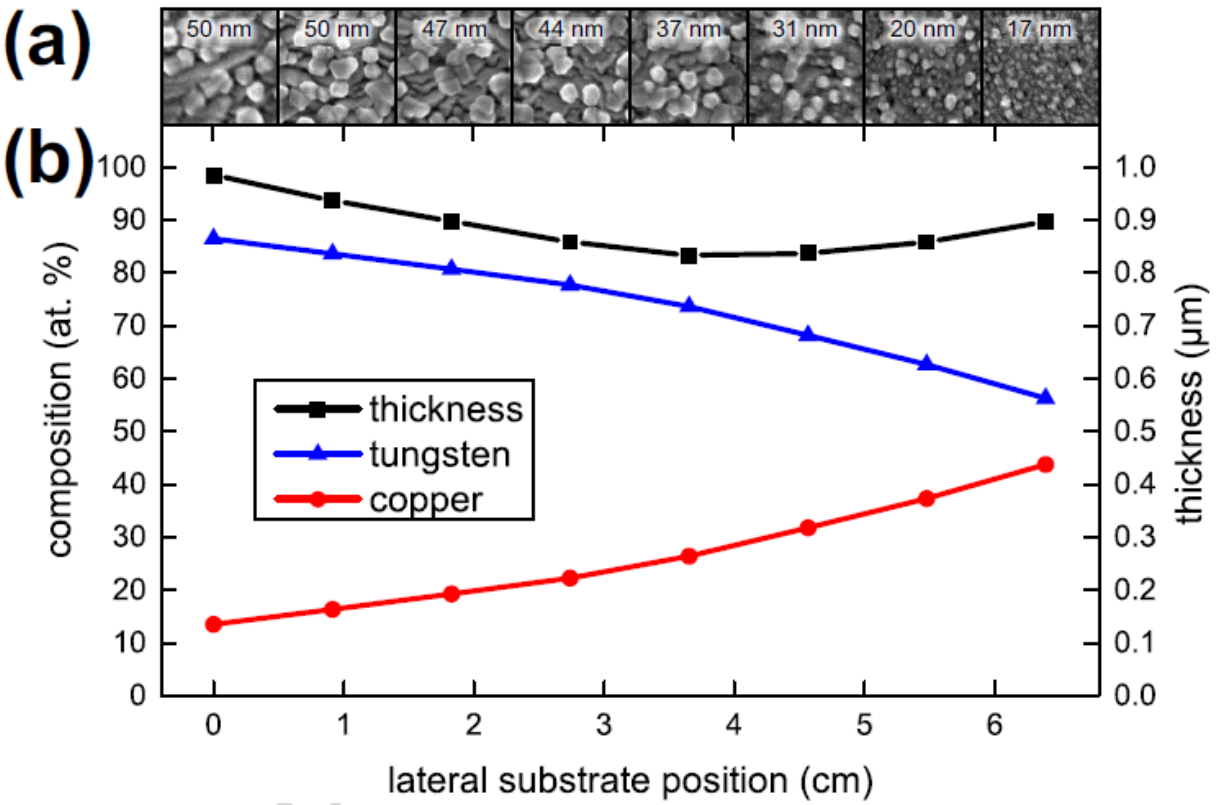

Figure 2: (a) Offset logarithmic plot of XRD scans from 30° to 110° consistent with a single BCC phase with no significant change in texture with changing chemical composition (b) Detailed scans from 39° to 44° with continuous variation in the diffraction angle and intensity of the {110} diffraction peak. Three sites diffract more strongly than the others, indicating enhanced long-range order at these chemical compositions.

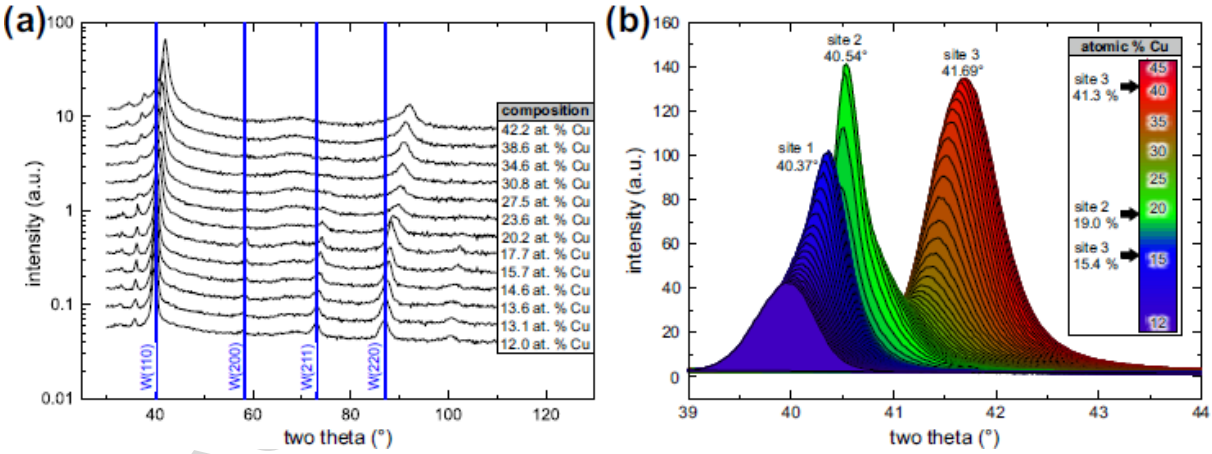

Figure 3: (a) BFTEM (b) SAD patterns and (c) radially integrated SAD intensity at the three chemical compositions for which the strongest X-ray diffraction was observed

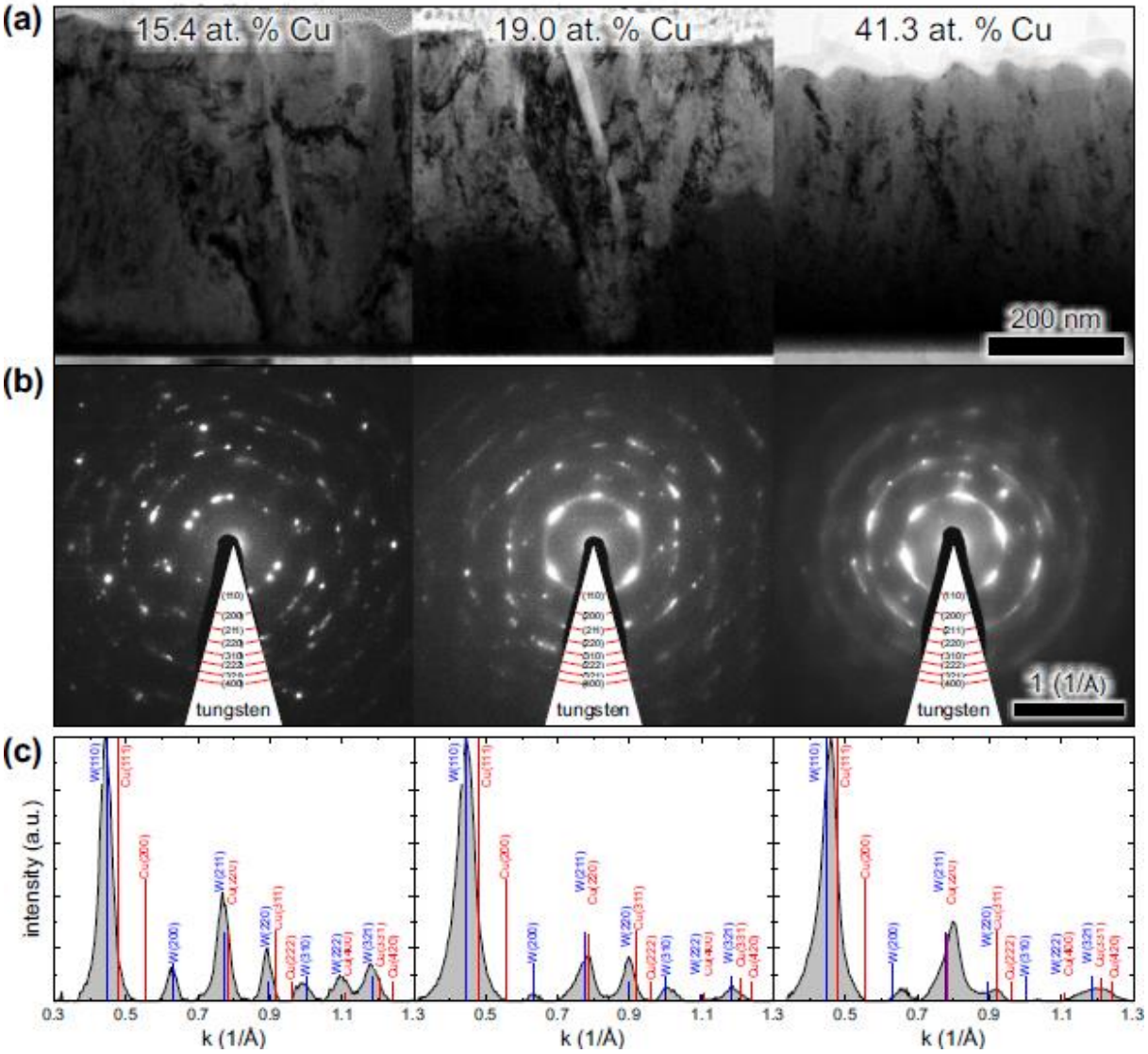

Figure 4: (a) Hardness and (b) reduced modulus of Cu-W compositional gradient film together with rule of mixture fits calculated from the measured values of pure copper and pure tungsten

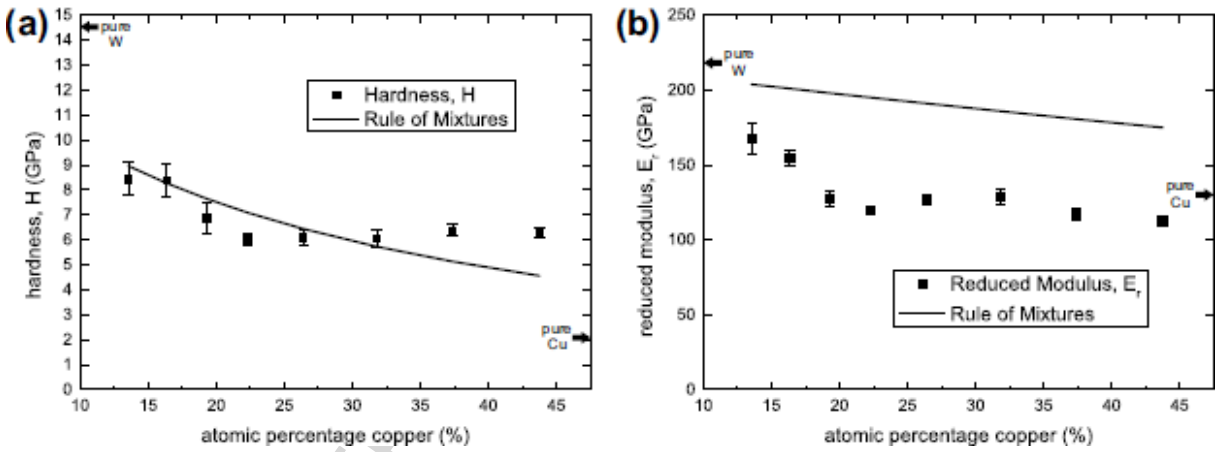

Figure 5: (a) Plane spacing and (b) crystallite size calculated using the Scherrer equation and the data from the detailed XRD scans seen in Figure 2(b)

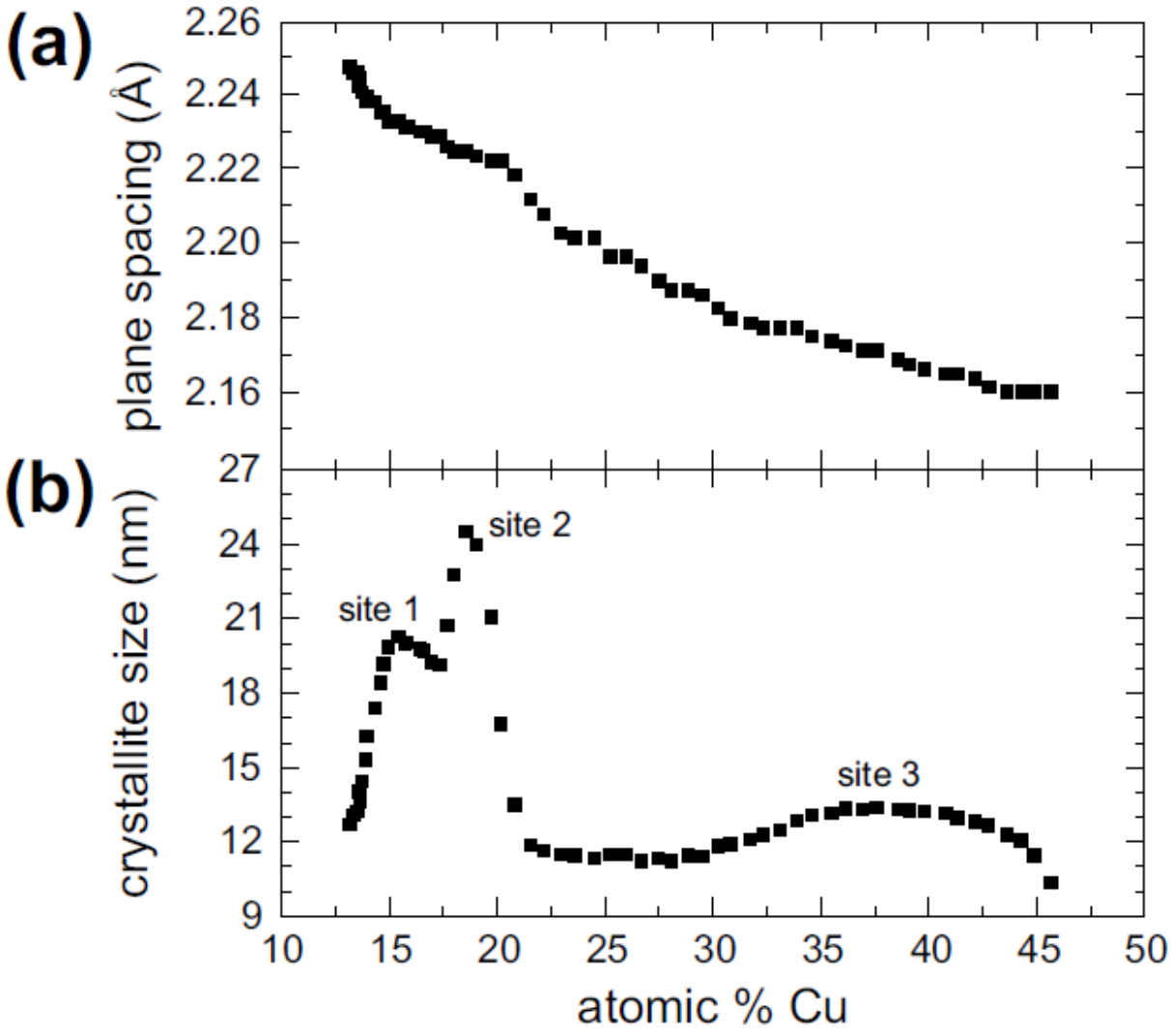

Figure 6: Calculated hardness contributions for Hall-Petch (grain boundary), Fleischer (solid solution), and Rupert (nanocrystalline solid solution) strengthening models together with measured film hardness

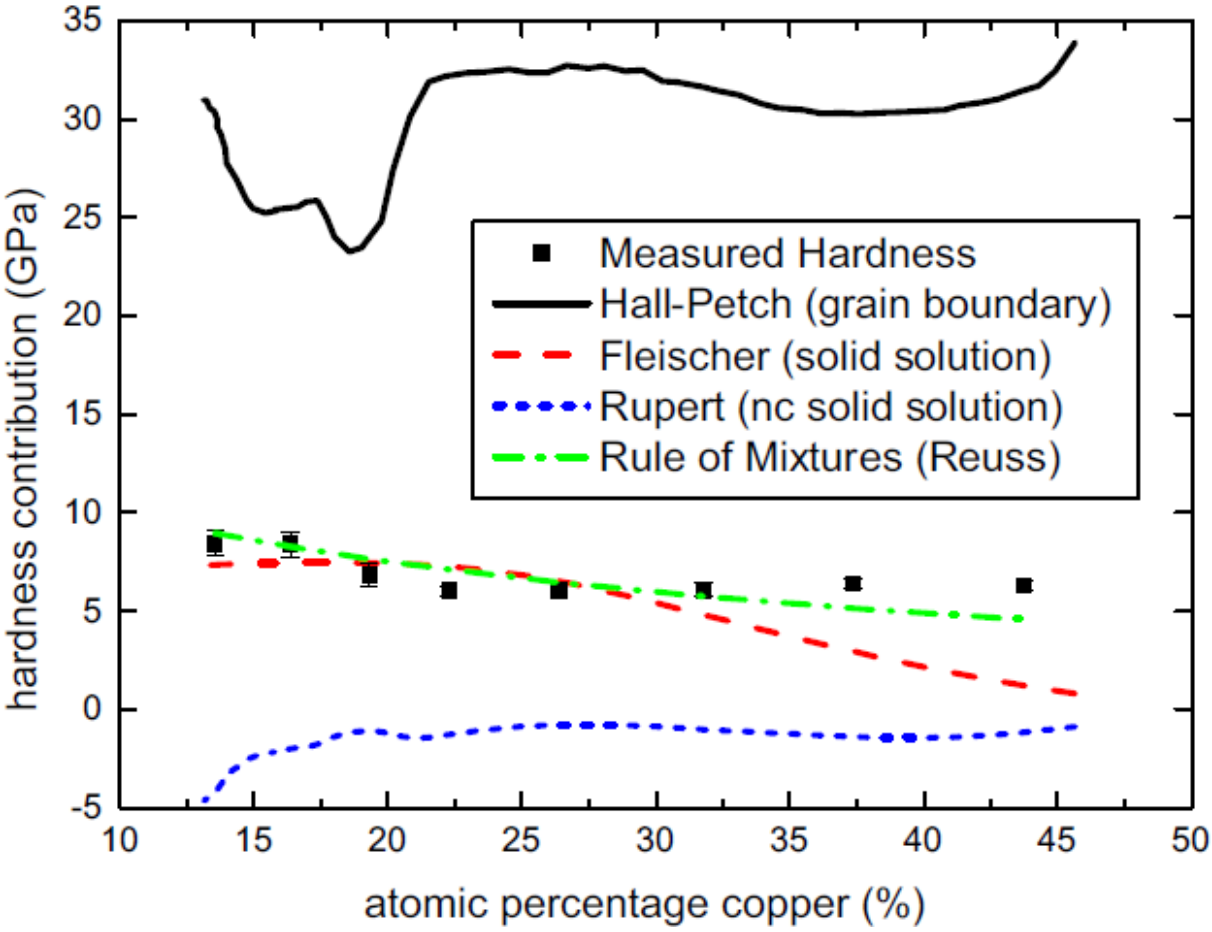

Highlights

- A combinatorial approach is used to study a metastable Cu-W solid solution
- A lateral compositional gradient is achieved through co-sputtering
- Three chemical compositions exhibit enhanced X-ray diffraction
- Available strengthening models do not accurately predict the film’s hardness